Friction on I-Modified Au(111) in a Tetraglyme Electrolyte

Inhee Park,[a] Florian Hausen,[b, c] and Helmut Baltruschat*[a]

In situ electrochemical lateral force microscopy (EC-LFM) has been employed to study the ordered structure of Li^+ containing tetraglyme (G4) in front of I-modified Au(111) and its influence on friction as function of normal load. Since the effect of water in aprotic electrolytes is a critical issue, the influence of water on the ordered structure and friction was also been investigated. Lateral force maps recorded at low normal load ($F_N <$ 30 nN) show that the adsorbed iodine forms a $(\sqrt{3} \times \sqrt{3})R30^\circ$ structure ($\theta_I = 0.33$) independent of potential. With increasing normal load, observed atomic corrugations at both potentials (0.45 V and −0.4 V) are in agreement with the Au(111) (1×1) structure while returning to a $(\sqrt{3} \times \sqrt{3})R30^\circ$ structure with decreasing normal load. Thus we conclude that the AFM tip penetrates into the iodine adlayer without irreversible wear. Astonishingly, no clear friction increase was observed upon penetration into the iodine adlayer; also no corresponding step was found in force separation (FS) curves. On the other hand, FS curves for I-modified Au(111) in pure G4 solvent and Li^+ containing electrolyte clearly showed several steps suggesting that G4 molecules are forming up to five ordered layers. It is noteworthy that we observed two different push-through forces for the innermost layers. Considering the higher reproducibility of FS curves on I-modified Au(111) compared to bare Au(111) we assume that the low surface energy of the iodine monolayer leads to negligible interaction between G4 molecules and iodine adlayer, resulting in less perturbations of the structure by the solid phase and also an increase of push-through force. Charts of friction forces vs. normal load are found to be independent of applied potential and the concentration of water.

Introduction

Friction between two surfaces is an important issue in everyday life and is the ultimate cause of all mechanical energy dissipation. Understanding its origin, finding factors that influence it, and ways to reduce it is therefore of extreme importance. Friction often occurs in a liquid environment (or wet or lubricated surfaces) and hence, electrochemistry is involved. Here we will study the interaction between a sliding or static AFM tip serving as a model for a single asperity and an iodine covered Au(111) surface in an aprotic tetraglyme electrolyte. Since iodine is known to be very strongly adsorbed, the latter is an ideal, comparatively simple model system.

Numerous studies of atomic scale friction employed atomic force microscopy or lateral force microscopy (AFM or LFM),[1–12] a technique that is also well suited to elucidate the lateral atomic structure.[13] As compared to the electrochemical scanning tunneling microscopy (EC-STM),[14,15] it has the disadvantage of a typically lower lateral resolution. However, AFM has the advantage that, by recording tip approach curves (force separation (FS) curves), also information on structuring of the electrolyte or solvent normal to the surface can be obtained.[16–19] Such an information on both lateral and vertical structure is important for an understanding of all kinds of electrode processes and catalytic reactions. It is also obvious that vertical interaction potentially influence friction forces.

O'Shea et al. have reported FS curves on highly oriented pyrolytic graphite (HOPG) in binary liquid mixture composed with octamethylcyclotetrasiloxane (OMCTS) and squalene (or hexadecane) using an AFM.[20] Results show that the affinity between surface and molecule determines the innermost layer. The hydration layer at the interface with substrates has been elucidated using a high-resolution frequency modulation atomic force microscope (FM-AFM).[17,21,22] These results suggest that the surface property (solvophilicity vs. solvophobicity) might influence the packing density of hydration layer at the interface. The interfacial structures between solid surfaces of electrodes and ionic liquids (ILs) have shown that the ordered layers composed of ions are modified by applied potential due to the rearrangement of ions.[18,23–25] Solvate ionic liquids (SILs) consisting of an equimolar mixture of organic lithium salts and glymes (e.g. triglyme (G3), tetraglyme (G4)) have found interest in similar studies because of their similar behavior as ILs (e.g. low volatility, high thermal stability, high ionic conductivity, and a wide potential window).[26–31] McLean et al. reported force separation curves on highly ordered pyrolytic graphite (HOPG) and Au(111), which varies with the anion of lithium salts and the applied potential due to the rearrangement of ions.[28] We are not aware of similar studies for organic electrolyte systems other than ILs, in particular aprotic electrolytes.

[a] I. Park, Prof. Dr. H. Baltruschat
Institute of Physical and Theoretical Chemistry
University of Bonn
Römerstr. 164, 53117 Bonn, Germany
E-mail: Baltruschat@uni-bonn.de
[b] Prof. Dr. F. Hausen
Institute of Energy and Climate Research, IEK-9 – Fundamental Electrochemistry Forschungzentrum Jülich GmbH
52425 Jülich, Germany
[c] Prof. Dr. F. Hausen
Institute of Physical Chemistry
RWTH Aachen University
Landoltweg 2, D-52074 Aachen, Germany

Supporting information for this article is available on the WWW under https://doi.org/10.1002/celc.202101660

Such FS curves may also be determined using surface forces apparatus (SFA, or surface force balance, SFB). Christenson et al. have reported such FS curves in nonpolar liquids (e.g. OMCTS, cyclohexane, benzene).[32–34] The results revealed that the number of measurable oscillations decreases with increasing molecular flexibility (e.g. rotation, asymmetry) as flexible molecules are able to pack effectively without layering. Interestingly, with adding small amounts of water in OMCTS, oscillatory forces disappear due to the strong adsorption of water on the mica surface.[35] Perkin et al. have found an oscillatory behavior when squeezing out layers of ionic liquids (ILs) on mica.[31,36,37]

Coming back to friction, the AFM tip is ideally suited to model a single asperity of a rough surface moving across another surface. In electrolyte solutions, friction is influenced by the lubricating effect of the electrolyte, as well as that of adsorbates. In addition, the electrode potential may have a direct or an indirect (by influencing adsorption processes) impact on friction. Therefore, apart from the importance of friction on wet surfaces (and thus electrodes), electrochemistry also offers means to control friction.[1–12] For SILs, Li et al. demonstrated that friction as function of normal load correlates with the interaction between ions and the surface by varying potential. Furthermore, they observed that the behavior of friction with potential depends on substrate (HOPG and Au-(111)).[29] However, it is still unclear why the dependence of friction closely related to the arrangement of ions shows a difference between HOPG and Au(111).

To simplify the system, we exclude coverage effects of adsorbate on friction[38] by modifying surface of Au(111) with an iodine adlayer.[14,22,39–48] We demonstrate that the AFM tip can penetrate into the iodine adlayer without irreversible wear as normal load increases. The electrochemical window is chosen such that no electrochemical reaction occurs. As solvent, tetraethylene glycol dimethyl ether (G4) is used to exclude hydrogen bonding that might influence friction. This aprotic electrolyte also seemed interesting because of the similarity to the above mentioned SILs. Finally, the electrochemistry in this electrolyte is important because such ether-based electrolytes have been studied as an alternative electrolyte for the Li-O_2 battery due to their greater stability during oxygen reduction reaction (ORR) compared with organic carbonate-based electrolytes (e.g. propylene carbonate (PC)).[49–51] G4 is also of interest for application as an electrolyte solvent for Mg deposition-dissolution processes.[52–57]

Questions to be answered in this study are: Do G4 molecules order near the surface of an I-modified Au(111) electrode as in the above mentioned examples for SILs. Furthermore, would the squeezing out the innermost layer of G4 molecules have an influence on friction? Also of interest is if the tip penetration into the iodine adlayer could be observed in FS curves and whether this tip penetration leads to an increase or change of friction, as one might expect from previous studies.[37,58,59] Two different kinds of experiments are performed with the AFM: either measurement of friction (lateral force) when the tip is laterally moving (perpendicular to the cantilever) or force distance curves for a fixed x-y position of the tip.

Material and Methods

A disc-type Au(111) single crystal (diameter: 10 mm and thickness: 3 mm) purchased from MaTecK GmbH (Germany) was used as working electrode. It was annealed by flame and cooled down above iodine crystals purged with Ar, forming a monolayer of iodine on clean surface. In the H-cell, a gold wire was used as counter electrode and silver wire in 2 mM $AgClO_4$/0.1 M $LiClO_4$/G4 was used as reference electrode. In the AFM-cell, gold and silver wires were used as counter and quasi reference electrode, respectively. For electrolytes, 0.1 M $LiClO_4$ were dissolved in tetraethylene glycol dimethyl ether (G4). A coulometric KF Titrator (C20, Metler Toledo) with a diaphragm electrode was used to measure the water content.

Lateral (frictional) force measurements were performed using Agilent 5500 AFM, combined with an atmosphere chamber. Silicon tips (PPP-FM, NANOSENSORS, tip radius <10 nm) were used and the normal spring constant was individually calibrated to 1.1 ± 0.05 N/m. Normal and torsional resonance frequency of AFM tips were measured by AFM (Agilent 5500/AC mode). The Q factor for theses resonance frequencies was obtained by fitting the equation of simple harmonic oscillation (SHO).[60] Normal and torsional force constants were calculated using the Sader method[60,61] and the lateral force constant was obtained by dividing torsional force constant with the square of the tip height. During the measurement, a homemade AFM cell was used, which contains a three-electrode assembly and Ar was purged through the atmosphere chamber. The lateral force vs. normal load and potential curves were measured using the silicon tip, PPP-FM, and the scan size and rate were 20 nm^2 and 0.47 nm/s, respectively.

When the AFM tip scans the surface, friction (F) between the tip and surface makes the cantilever twist, which results in the deflection of the laser beam. The sign of the deflection depends on the scan direction. In addition, the deflection of the laser can be caused by topography (T) (e.g. steps on the surface) and it does not depend on scan direction. Thus, the forward image and backward image contain [T+F] and [T−F], respectively. Friction force data was obtained by subtracting the backward data from the forward data and dividing it by 2 to eliminate topographic effects.[62]

Atomic corrugations of the surface can be visualized in lateral force maps. To investigate structures in detail, the right or left side of the images are removed such that oscillations of the scan piezo during the change of scan directions do not disturb the image. Fast Fourier Transform (FFT) filtering was used in some images. The thermal drift was corrected by recording two subsequent images in downward and upward direction which allows calculating the drift vector.[63] The illustration of lattice shows the lattice parameters obtained after the correction of thermal drift. For highly oriented pyrolytic graphite (HOPG) in air, the discrepancy of atomic structures obtained using topography and lateral force map was negligible. Furthermore, the observed lattice parameters were approx. 10% larger than the theoretical value, mainly due to viscous effects and errors in thermal drift correction. Therefore, we assume that the experimental value contains basically ±10% error and it might be slightly larger under electrochemical conditions.

Force distance curves were typically repeated approx. ten times to ensure reproducibility.

Results and Discussion

Cyclic Voltammetry

Figure 1 shows the cyclic voltammogram (CV) obtained in an H-cell containing 0.1 M $LiClO_4$/G4 with trace amounts of water (21 ppm). In this potential range, where no chemical reaction occurs, the small cathodic peak, C_1, appears only in the first sweep. Since the potential range in this measurement is far positive from the desorption potential of iodide ($E = -1.2$ V vs. Ag/Ag^+)[47], it is assumed that C_1 is related to the desorption of a small amount of iodine exceeding the coverage of the ordered $(\sqrt{3} \times \sqrt{3})R30^\circ$ adlayer described below. Figure S1 shows the second cycle of CV in AFM-cell verifying that the concentration of water has no large influence on electrochemical reaction on I-modified Au(111).

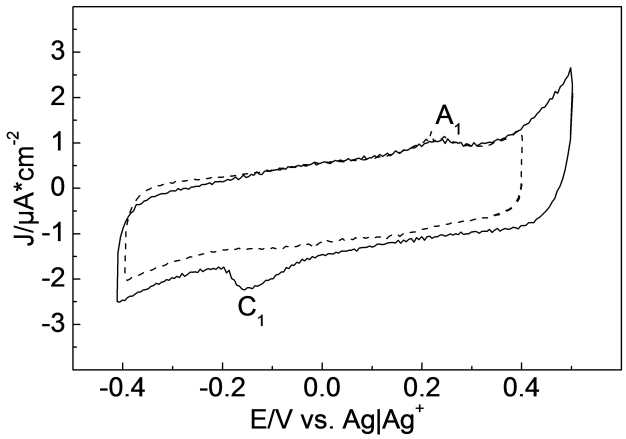

Figure 1. Cyclic voltammogram of I-modified Au(111) in 0.1 M $LiClO_4$/G4 in H-cell. Solid line and dashed line indicate the 1st and 2nd sweep, respectively. The amount of water in electrolyte is about 21 ppm. The sweep rate is 50 mV/s.

Atomic Corrugation

At relatively low normal load ($F_N < 30$ nN), a $(\sqrt{3} \times \sqrt{3})R30^\circ$ structure is dominantly observed at both potential of $+0.45$ V and $\times 0.4$ V (vs. Ag/Ag^+) on I-modified Au(111) in 0.1 M $LiClO_4$/G4, indicating that the coverage of iodine is 0.33 (Figure 2) over the whole potential range; therefore, the small peak, C_1, observed in the first sweep of CV is not related to a phase transition. With increasing normal load above 50 nN, the revealed atomic corrugations correspond to a $Au(111)(1 \times 1)$ structure as shown in Figure 3. Therefore, we conclude that at a sufficiently high normal load the tip penetrates the iodine adlayer and this behavior (visibility of the iodine structure for $F_N < 30$ nN and of the gold structure for $F_N > 50$ nN) is independent of potential. No clear structure was observed for intermediate normal loads. Figure S2 directly shows the transition of the atomic stick-slip structure with increasing and decreasing normal load in one lateral force map for two different potentials: The $(\sqrt{3} \times \sqrt{3})R30^\circ$ structure is also observed, when the normal load is reduced again. Obviously, this structural transition for changing normal loads is reversible. Therefore, we presume that there is no, or at least no irreversible wear, possibly due to strong interaction between iodine and the surface of Au(111).

It is interesting to note that the 'stick-slip lateral force loops' show no energy dissipation for low normal loads (cf. Figure 4). This is expected according to the Tomlinson model as described in Refs.[64,65] this will be discussed in more detail in a forthcoming paper.

On bare Au(111) in 0.1 M $LiClO_4$/G4, atomic corrugation consistently shows the lattice structure of Au(111) at low and high normal loads, as shown in Figure S3 together with the cyclic voltammetry in the AFM-cell. As for I-modified Au(111), in the potential range between -0.4 V to 0.45 V there was no electrochemical reaction. This result confirms that the transition

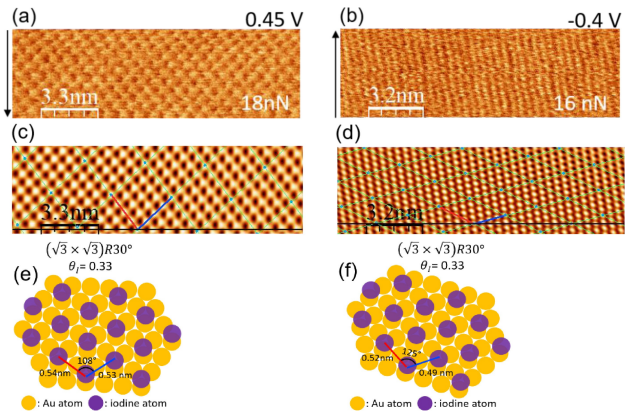

Figure 2. Lateral force maps at (a) 0.45 V (vs. Ag/Ag+) and (b) −0.4 V. (c) and (d) are the lattice images after Fast Fourier Transform (FFT) of (a) and (b), respectively. (e) and (f) are the illustration of the real lattice with lattice parameters after the correction of thermal drift. Applied normal loads of (a) and (b) are 18 nN and 16 nN, respectively. The water concentrations of (a) and (b) in the electrolyte are 21 ppm and 100 ppm, respectively. Scan rate is 0.47 nm/s.

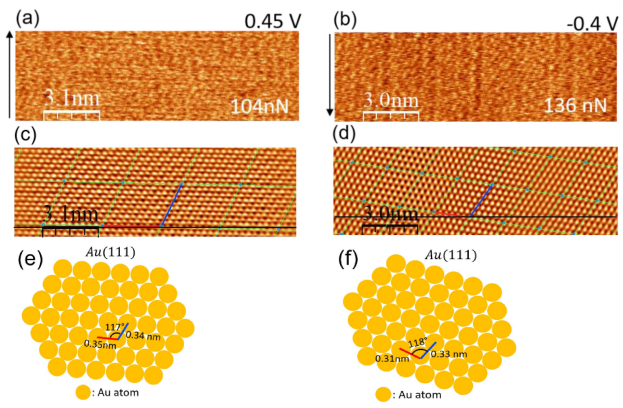

Figure 3. Lateral force maps at (a) 0.45 V (vs. Ag/Ag+) and (b) −0.4 V. (c) and (d) are the lattice images after Fast Fourier Transform (FFT) of (a) and (b), respectively. (e) and (f) are the illustration of the real lattice with lattice parameters after the correction of thermal drift. Applied normal loads of (a) and (b) are 104 nN and 136 nN, respectively. The water concentrations of (a) and (b) in the electrolyte are 21 ppm and 100 ppm, respectively. Scan rate is 0.47 nm/s.

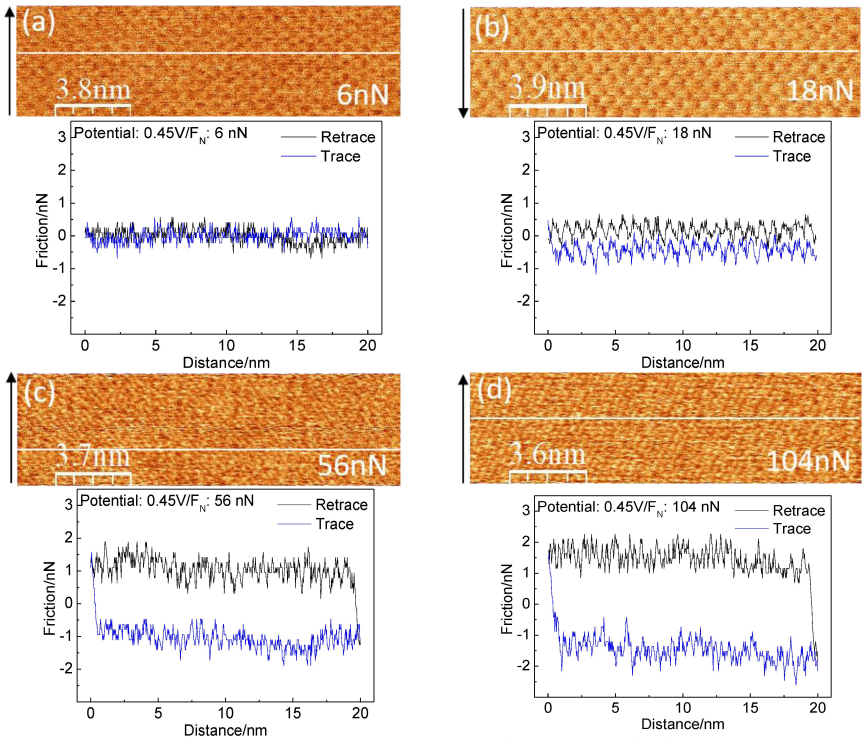

Figure 4. Lateral force loops at 0.45 V and stick-slips at the normal load of (a) 6 nN, (b) 18 nN, (c) 56 nN, and (d) 104 nN. The water concentration is 21 ppm. Scan rate is 0.47 nm/s.

of structures is caused by the penetration of AFM tip into the iodine adlayer.

As shown in Figure S4 and S5, an increased water content (300 ppm) in the electrolyte has no influence on the structure of adsorbed iodine and the penetration of tip into this adlayer at high normal load.

Interfacial Structure: Ordered Solvent Layers on the Surface

To further probe the penetration of the iodine adlayer, FS curves have been acquired. FS curves are recorded at 0.45 V and −0.4 V on I-modified Au(111) for different concentrations of water in the electrolyte. Typical FS curves are shown in Figure 5. A clear layering structure is revealed by the stepwise increase of normal force upon approach. Ordered layers of electrolyte require an additional force for disruption by the AFM tip moving toward the surface, resulting in discrete steps in FS curves.[16] The force required to rupture a layer is referred to as the 'push-through force'.[30]

Zero force is measured beyond 5 nm from the surface, revealing that there the electrolyte acquires its bulk structure. As the AFM tip moves closer to the surface, several layers are detected regardless of applied potential. The highest push through force observed was ~5 nN. Even though the applied normal load was increased to 50 nN, there was no further step indicating a higher push-through force, although with this normal load the lattice structure of the substrate always appeared. Therefore, we presume that there is no penetration of the iodine layer by the tip during recording of the tip approach curves and thus no displacement of iodine. Probably, in addition to a high normal load a sufficient shear force might be required: The normal force provides the necessary (thermodynamic) energy for desorption and displacement of the iodine, whereas the lateral shear force helps to overcome the kinetic energy barrier for the penetration into the iodine adlayer.[66] This barrier might be rather high because desorption has to happen for a large number of atoms simultaneously.

Interestingly, no effect of the amount of water in the electrolyte was found. Christenson et al. reported that the oscillations disappear when small amounts of water were added to nonpolar liquids due to the preferred adsorption of water on the mica surface.[32,67] In contrast to this observation, the hydrophobic character of the adsorbed iodine adlattice in the system studied here prevents the incorporation of water to the interface. It is worth noting that the observed FS curves on bare Au(111) in the same electrolyte show no clear steps. Therefore, it is rather probable that adsorption and structured layering of G4 molecules is preferred on hydrophobic I-modified Au(111).

The push-through force for outer layers is relatively small and independent of the applied potential but the distance of outer layers is slightly smaller at −0.4 V (~0.44 nm) than 0.45 V (~0.6 nm). Figure S6 shows FS curves obtained on I-modified Au(111) in pure G4. The similarity to those obtained in presence of electrolyte suggests that the ordered layers are mostly attributed to G4 molecules preferentially oriented parallel to the surface of I-modified Au(111).[30] The slight decrease of the layer thickness with decreasing distance suggests that the G4

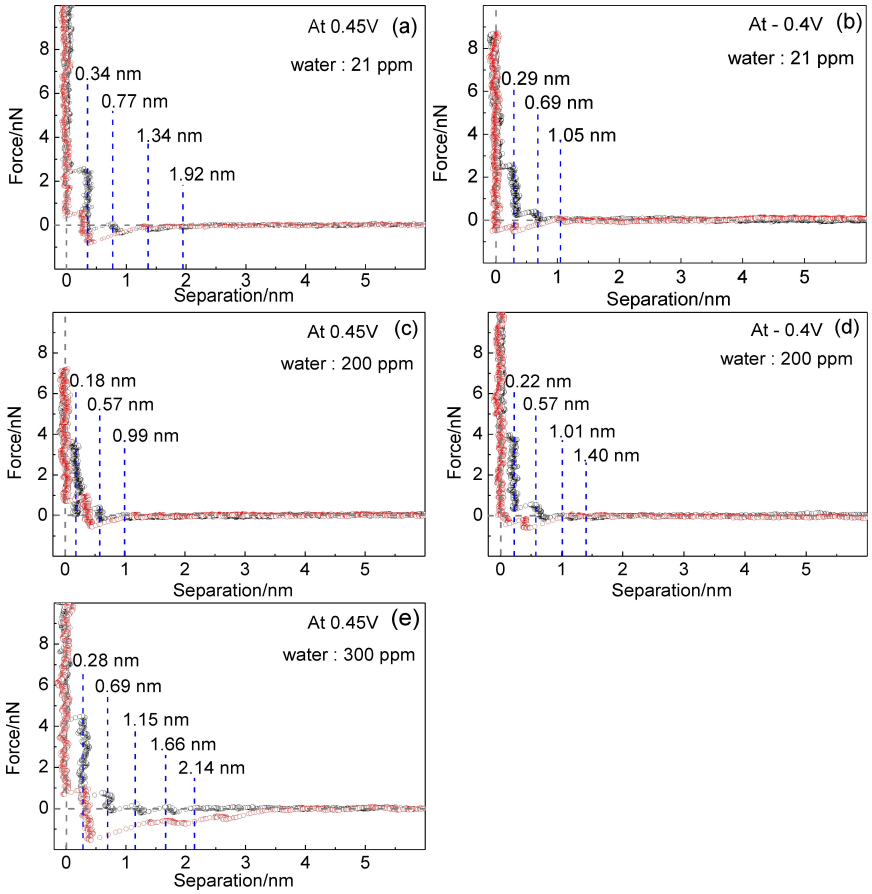

Figure 5. Force separation profiles obtained on the I-modified Au(111) in 0.1 M $LiClO_4$/G4 containing water (a) and (b) 21 ppm, (c) and (d) 209 ppm, and (e) 300 ppm. The applied potential for (a), (c), and (e) is 0.45 and for (b) and (d) is −0.4 V. All profiles show the approach of AFM tip to the working electrode and approaching speed of tip is 80±10 nm/s.

molecules are somewhat flexible and can be compressed by the AFM tip, leading to a slightly increased ordering or packing density.[20,67] It therefore is not surprising that the thickness of the innermost layer also varies a little with potential. The force required to rupture layers increases as the separation decreases as is often observed (Figure 5 and Figure S6a).[20,30,67] We assume that the low surface energy of the iodine monolayer leads to a very low interaction with the G4 molecules of the liquid. This solvophobic behavior results in less perturbations of the G4 liquid surface structure by the solid iodine covered Au(111) surface. The required push-through force corresponds to the energy necessary for a disrupture of the ordered liquid layer. This also explains the lower reproducibility of FS curves on bare Au(111), where the stronger interaction of the G4 molecules with the surface prevents such an ordering. It is instructive to compare the energy required to break the innermost layer with the tip calculated using our data from Figure 5 (layer thickness: 0.3 nm and normal force: 3 nN) which is about 0.9×10^{-18} N·m with that calculated from the surface tension. From the surface tension of G4 of 34×10^{-3} N/m[68] and the estimated surface area of the tip of 2.8×10^{-17} m^2 we obtain an energy of 0.95×10^{-18} N·m, which is closer than one could expect from the crude approximation. (For the calculation, we simply assumed that the contact surface is a flat circle with a radius of it is 3 nm. This supports our assumption that the interaction with the solvophobic iodine layer is negligible. Occasionally, a relatively large rupture force for the innermost layer (cf. Figure S6b and Figure S7) is observed. This suggests that the strength of the interaction between the iodine adlayer and G4 molecules is somewhat varying together with the liquid structure, possibly at defects of the surface.

As the AFM tip moves away from the surface the FS curves sometimes show clear steps, suggesting a fast reordering of G4 molecules on I-modified Au(111), but more often the adhesion force predominates (Figure S8).

Dependence of Friction on Normal Load

Although the classical friction law of Amontons predicts a linear relationship between friction and normal load, in electrochemical systems often a non-linear behavior is observed.[2,4,6] On electrode surfaces, a sudden increase in friction or a plateau region had been ascribed to the penetration of the tip into an ionic layer. Also in ionic liquids, such a sudden, stepwise increase in friction was observed upon penetration of the tip through distinct electrolyte layers; there, penetration was confirmed by force distance curves.[58,69] Therefore, since the

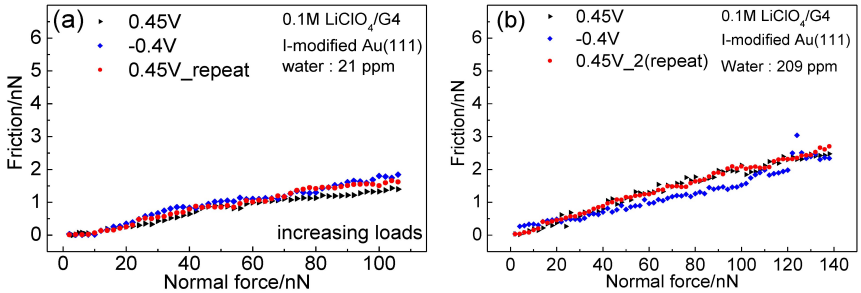

Figure 6. The dependence of friction on normal load at fixed potentials on I-modified Au(111) in 0.1 M $LiClO_4$/G4 containing (a) 21 ppm water and (b) 209 ppm water. The scan size and scan rate were 20×20 nm^2 and 0.47 nm/s, respectively.

atomically resolved LFM images (Figure S2) showed that the AFM tip penetrates into the iodine adlayer with increasing normal load, a similar stepwise friction increase might be expected also for the iodine modified Au(111) in G4.

Figure 6a shows friction force as function of normal load for I-modified Au(111) in 0.1 M $LiClO_4$/G4. No clear deviation from the classical linear relationship (Amontons' law) is observed. Furthermore, the slope, i.e. the friction coefficient, is independent of potential and found to be 0.02. However, according to the discussion above, it is astonishing that there is no clear abrupt change of friction after the penetration of the tip into the iodine adlayer, when the tip is in contact with the Au(111) substrate. Obviously, the friction coefficient for the iodine covered surface and for the Au substrate are similar. A control experiment on a pure, i.e. iodine free Au(111) electrode shows that this is indeed the case: the resulting friction vs. normal load curve is very similar (Figure S9). The similarity of energy dissipation and friction before and after penetration of the iodine layer therefore suggests that the iodine within the adsorbate layer is quite mobile. The independence of friction of applied potential also suggests that the adsorption strength of iodine on Au(111) (which should vary with potential) is not a decisive factor. This is opposed to the case of adsorbed sulfate, for which we assumed desorption and readsorption during scanning of the tip,[2] whereas iodine atoms are only laterally shifted, always staying in contact with the Au surface. The value of the surface diffusion barrier, which may also depends on potential, seems to be too low to play a role. This does not contradict the fact that iodine is strongly adsorbed: The energy barrier for surface diffusion is completely independent of that for desorption.

In Figure 6a, friction remains nearly zero up to a normal load of 10 nN. This is consistent with the fact that the lateral force loop on the iodine adlayer also shows the expected transition from continuous movement without energy dissipation to stick-slip motion with an additional energy dissipation around 10 nN as shown in Figure 4.[64,65]

Figure 6b shows the friction results when the amount of water in the electrolyte is raised to 209 ppm. Again, friction increases linearly with normal load, independent of potential and resembles the results as shown in Figure 6a for a water content of 21 ppm. This result demonstrates that even after the penetration of the iodine adlayer, the water has a minor influence on friction forces.

Conclusions

We investigated the frictional behavior of I-modified Au(111) for different potentials and normal loads. At low normal loads ($F_N <$ 30 nN), the atomic structures show that the adsorbed iodine atoms form a $(\sqrt{3}\times\sqrt{3})R30°$ adlattice at both potentials. At high normal loads, ($F_N > 50$ nN), the revealed LFM structure and atomic stick-slip indicate that the tip slides directly on the Au(111) surface. It is noteworthy that with increasing normal load, the AFM tip penetrates into iodine layer without irreversible wear. Such structural image changes are often observed in STM when increasing the setpoint of the tunneling current.[14,70,71] However, we are not aware of similar structural transitions observed by AFM upon increasing load. FS curves show that several ordered solvent layers (~5 layers) are formed in the electrolyte in front of I-modified Au(111) independent of potential and the amount of water. The stepwise push-through forces and distance between layers resemble the results observed in pure G4. Therefore, the vertically ordered layers on I-modified Au(111) are attributed to G4 molecules. Considering that we did not observe clear stepwise FS curves on bare Au(111), we assume that the lower surface energy of the iodine monolayer leads to negligible interaction between G4 molecules and iodine adlayer. Thus, G4 molecules form stable ordered layers to minimize the surface energy of the liquid phase and that of the interface. Two different push-through forces for the innermost layer may indicate different ordering. These forces seem to be too small to show up in the friction vs. load curves. In the present measurements, the effect of water was negligible, in contrast to previous reports in literature.[32,33] A reasonable assumption is that due to the unfavorable adsorption of water on the hydrophobic iodine adlayer, water has no influence on the arrangement of G4 molecules.

Astonishingly, we did not observe a push-through force corresponding to the structural change and the penetration of the tip into the iodine adlayer. It seems that a larger push though force is needed in the absence of a lateral tip movement. The dependence of friction forces as function of normal load shows a monotonic increase independent of potential and

the concentration of water. This implies that the strength of the iodine adsorbed on Au(111) has no variation with potential in this potential region and it is a minor effect on friction. Moreover, a stepwise increase of friction upon increasing the normal load and upon the structural transition caused by penetration of the tip into either solvent layers or the adsorbate layer, as found in other cases,[2,4,6,58,69] was not observed. Therefore we assume that the adsorbed iodine is quite mobile, and no extra energy is dissipated to push it away in front of the sliding tip.

Acknowledgment

The authors gratefully acknowledge the DFG (Deutsche Forschungsgemeinschaft) for funding this work (BA1008/21-1). Open Access funding enabled and organized by Projekt DEAL.

Conflict of Interest

The authors declare no conflict of interest.

Data Availability Statement

The data that support the findings of this study are available in the supplementary material of this article.

Keywords: electrolyte structure · tribology · atomic force microscopy · lateral force microscopy · force separation curve

[1] M. Nielinger, H. Baltruschat, *Phys. Chem. Chem. Phys.* **2007**, *9*, 3965–3969.
[2] F. Hausen, M. Nielinger, S. Ernst, H. Baltruschat, *Electrochim. Acta.* **2008**, *53*, 6058–6063.
[3] M. Nielinger, F. Hausen, N. Podghainiy, H. Baltruschat in *Nanotribology at electrodes: Influence of adsorbates and potential on friction forces studied with atomic force microscopy*, Vol. (Eds.: A. Fischer, K. Bobzin), Wiley-VCH, Weinheim, **2009**, pp.178–184.
[4] N. Podgaynyy, S. Iqbal, H. Baltruschat, *Surf. Sci.* **2015**, *631*, 67–72.
[5] N. Podgaynyy, S. Wezisla, C. Molls, H. Baltruschat, *Beilstein J. Nanotechnol.* **2015**, *6*, 820–830.
[6] I. Park, H. Baltruschat, *ChemPhysChem.* **2021**, *7*, 1–9.
[7] N. N. Gosvami, T. Filleter, R. Bennewitz, *Tribol. Lett.* **2010**, *39*, 19–24.
[8] A. Labuda, W. Paul, B. Pietrobon, R. B. Lennox, P. H. Grutter, R. Bennewitz, *Rev. Sci. Instrum.* **2010**, *81*, 083701.
[9] A. Labuda, F. Hausen, N. N. Gosvami, P. H. Grütter, R. B. Lennox, R. Bennewitz, *Langmuir.* **2011**, *27*, 2561–2566.
[10] F. Hausen, N. N. Gosvami, R. Bennewitz, *Electrochim. Acta.* **2011**, *56*, 10694–10700.
[11] R. Bennewitz, F. Hausen, N. N. Gosvami, *J. Mater. Res.* **2013**, *28*, 1279.
[12] F. Hausen, J. A. Zimmet, R. Bennewitz, *Surf. Sci.* **2013**, *607*, 20–24.
[13] A. A. Gewirth, V. B. Elings, J. Massie, P. K. Hansma, S. Manne, *Science.* **1991**, *251*, 183–186.
[14] B. C. Schardt, S. L. Yau, F. Rinaldi, *Science.* **1989**, *243*, 1050–1053.
[15] R. Vogel, I. Kamphausen, H. Baltruschat, *Ber. Bunsen-Ges.* **1992**, *96*, 525.
[16] R. Lim, S. O'Shea, *Phys. Rev. Lett.* **2002**, *88*, 246101.
[17] K.-I. Fukui, T. Utsunomiya, Y. Yokota, *Jpn. J. Appl. Phys.* **2017**, *56*, 08LA03.
[18] H. Li, F. Endres, R. Atkin, *Phys. Chem. Chem. Phys.* **2013**, *15*, 14624–14633.
[19] J.-W. Yan, Z.-Q. Tian, B.-W. Mao, *Curr. Opin. Electrochem.* **2017**, *4*, 105–111.
[20] R. Y. Lim, S. O'Shea, *Langmuir.* **2004**, *20*, 4916–4919.
[21] K. Suzuki, N. Oyabu, K. Kobayashi, K. Matsushige, H. Yamada, *Appl. Phys. Express.* **2011**, *4*, 125102.
[22] T. Utsunomiya, S. Tatsumi, Y. Yokota, K.-I. Fukui, *Phys. Chem. Chem. Phys.* **2015**, *17*, 12616–12622.
[23] R. Hayes, G. G. Warr, R. Atkin, *Phys. Chem. Chem. Phys.* **2010**, *12*, 1709–1723.
[24] J. Sweeney, F. Hausen, R. Hayes, G. B. Webber, F. Endres, M. W. Rutland, R. Bennewitz, R. Atkin, *Phys. Rev. Lett.* **2012**, *109*, 155502.
[25] N. Borisenko, A. Lahiri, G. Pulletikurthi, T. Cui, T. Carstens, J. Zahlbach, R. Atkin, F. Endres, *Faraday Discuss.* **2017**, *206*, 459–473.
[26] K. Yoshida, M. Nakamura, Y. Kazue, N. Tachikawa, S. Tsuzuki, S. Seki, K. Dokko, M. Watanabe, *J. Am. Chem. Soc.* **2011**, *133*, 13121–13129.
[27] K. Dokko, N. Tachikawa, K. Yamauchi, M. Tsuchiya, A. Yamazaki, E. Takashima, J.-W. Park, K. Ueno, S. Seki, N. Serizawa, *J. Electrochem. Soc.* **2013**, *160*, A1304.
[28] B. McLean, H. Li, R. Stefanovic, R. J. Wood, G. B. Webber, K. Ueno, M. Watanabe, G. G. Warr, A. Page, R. Atkin, *Phys. Chem. Chem. Phys.* **2015**, *17*, 325–333.
[29] H. Li, M. W. Rutland, M. Watanabe, R. Atkin, *Faraday Discuss.* **2017**, *199*, 311–322.
[30] A. Cook, K. Ueno, M. Watanabe, R. Atkin, H. Li, *J. Phys. Chem. C.* **2017**, *121*, 15728–15734.
[31] S. W. Coles, M. Mishin, S. Perkin, M. V. Fedorov, V. B. Ivaništšev, *Phys. Chem. Chem. Phys.* **2017**, *19*, 11004–11010.
[32] H. Christenson, R. Horn, J. Israelachvili, *J. Colloid Interface Sci.* **1982**, *88*, 79–88.
[33] H. K. Christenson, *J. Chem. Phys.* **1983**, *78*, 6906–6913.
[34] H. K. Christenson, C. E. Blom, *J. Chem. Phys.* **1987**, *86*, 419–424.
[35] R. Horn, D. Evans, B. Ninham, *J. Phys. Chem.* **1988**, *92*, 3531–3537.
[36] S. Perkin, T. Albrecht, J. Klein, *Phys. Chem. Chem. Phys.* **2010**, *12*, 1243–1247.
[37] A. M. Smith, K. R. J. Lovelock, N. N. Gosvami, T. Welton, S. Perkin, *Phys. Chem. Chem. Phys.* **2013**, *15*, 15317–15320.
[38] W. Ouyang, A. S. de Wijn, M. Urbakh, *Nanoscale.* **2018**, *10*, 6375–6381.
[39] R. Oelgeklaus, J. Rose, H. Baltruschat, *J. Electroanal. Chem.* **1994**, *376*, 127–133.
[40] F. Lu, G. N. Salaita, H. Baltruschat, A. T. Hubbard, *J. Electroanal. Chem.* **1987**, *222*, 305–320.
[41] J. Albers, H. Baltruschat, I. Kamphausen, *J. Electroanal. Chem.* **1995**, *395*, 99–105.
[42] N. J. Tao, S. M. Lindsay, *J. Phys. Chem.* **1992**, *96*, 5213–5217.
[43] W. Haiss, J. K. Sass, X. Gao, M. J. Weaver, *Surf. Sci.* **1992**, *274*, L593-L598.
[44] B. M. Ocko, J. Wang, G. M. Watson, *J. Phys. Chem.* **1994**, *98*, 897–906.
[45] T. Yamada, N. Batina, K. Itaya, *Surf. Sci.* **1995**, *335*, 204–209.
[46] X. P. Gao, M. J. Weaver, *J. Am. Chem. Soc.* **1992**, *114*, 8544–8551.
[47] A. S. Shatla, P. P. Bawol, H. Baltruschat, *ChemElectroChem.* **2020**, *7*, 4782–4793.
[48] A. S. Shatla, A. A. Abd-El-Latif, S. Ayata, D. Demir, H. Baltruschat, *Electrochim. Acta* **2020**, *334*, 135556.
[49] S. A. Freunberger, Y. Chen, N. E. Drewett, L. J. Hardwick, F. Barde, P. G. Bruce, *Angew. Chem. Int. Ed. Engl.* **2011**, *50*, 8609–8613.
[50] R. Wen, M. Hong, H. R. Byon, *J. Am. Chem. Soc.* **2013**, *135*, 10870–10876.
[51] H. M. A. Amin, C. Molls, P. P. Bawol, H. Baltruschat, *Electrochim. Acta.* **2017**, *245*, 967–980.
[52] P. Hegemann, M. Hegemann, L. Zan, H. Baltruschat, *J. Electrochem. Soc.* **2019**, *166*, A245-A250.
[53] L. Zan, D. Xing, A. Abd-El-Latif, H. Baltruschat, *Beilstein J. Nanotechnol.* **2019**, *10*, 2541–2552.
[54] Da. Xing, P. P. Bawol, A.-E.-A. A. A. Abd-El-Latif, L. Zan, H. Baltruschat, *ChemElectroChem.* **2021**, *in press*.
[55] P. K. R. Kottam, S. Dongmo, M. Wohlfahrt-Mehrens, M. Marinaro, *Energies* **2020**, *13*, 1470.
[56] M. Marinaro, S. K. E. Moorthy, J. Bernhard, L. Jörissen, M. Wohlfahrt-Mehrens, U. Kaiser, *Beilstein J. Nanotechnol.* **2013**, *4*, 665–670.
[57] N. Amir, Y. Vestfrid, O. Chusid, Y. Gofer, D. Aurbach, *J. Power Sources.* **2007**, *174*, 1234–1240.
[58] H. Li, T. Niemann, R. Ludwig, R. Atkin, *J. Phys. Chem. Lett.* **2020**, *11*, 3905–3910.
[59] C. S. Perez-Martinez, S. Perkin, *Langmuir.* **2019**, *35*, 15444–15450.
[60] J. E. Sader, J. W. M. Chon, P. Mulvaney, *Rev. Sci. Instrum.* **1999**, *70*, 3967–3969.
[61] C. P. Green, H. Lioe, J. P. Cleveland, R. Proksch, P. Mulvaney, J. E. Sader, *Rev. Sci. Instrum.* **2004**, *75*, 1988–1996.
[62] S. Sundararajan, B. Bhushan, *J. Appl. Phys.* **2000**, *88*, 4825–4831.

[63] S. Iqbal, L. Zan, E. Nardi, H. Baltruschat, *Phys. Chem. Chem. Phys.* **2018**, *20*, 6176–6186.
[64] A. Socoliuc, R. Bennewitz, E. Gnecco, E. Meyer, *Phys. Rev. Lett.* **2004**, *92*, 134301.
[65] N. N. Gosvami, P. Egberts, R. Bennewitz, *J. Phys. Chem. A.* **2011**, *115*, 6942–6947.
[66] Z. B. Milne, R. A. Bernal, R. W. Carpick, *Langmuir.* **2019**, *35*, 15628–15638.
[67] H. Christenson, R. Horn, *Chem. Phys. Lett.* **1983**, *98*, 45–48.
[68] H. Manchanda, M. Kumar, *Renewables: Wind, Water, and Solar.* **2015**, *2*, 1–24.
[69] J. Sweeney, G. B. Webber, M. W. Rutland, R. Atkin, *Phys. Chem. Chem. Phys.* **2014**, *16*, 16651–16658.
[70] S. L. Yau, C. M. Vitus, B. C. Schardt, *J. Am. Chem. Soc.* **1990**, *112*, 3677–3679.
[71] P. Broekmann, M. Wilms, M. Kruft, C. Stuhlmann, K. Wandelt, *J. Electroanal. Chem.* **1999**, *467*, 307–324.

Manuscript received: December 15, 2021
Revised manuscript received: February 17, 2022
Accepted manuscript online: March 4, 2022